J Neurophysiol 114: 540–550, 2015.
First published May 20, 2015; doi:10.1152/jn.00360.2015.

Ambient illumination switches contrast preference of specific retinal processing streams

James T. Pearson[1,2] and Daniel Kerschensteiner[1,3,4]

[1]*Department of Ophthalmology and Visual Sciences, Washington University School of Medicine, St. Louis, Missouri;* [2]*Graduate Program in Developmental, Regenerative and Stem Cell Biology, Washington University School of Medicine, St. Louis, Missouri;* [3]*Department of Anatomy and Neurobiology, Washington University School of Medicine, St. Louis, Missouri; and* [4]*Hope Center for Neurological Disorders at Washington University School of Medicine, St. Louis, Missouri*

Submitted 10 April 2015; accepted in final form 18 May 2015

Pearson JT, Kerschensteiner D. Ambient illumination switches contrast preference of specific retinal processing streams. *J Neurophysiol* 114: 540–550, 2015. First published May 20, 2015; doi:10.1152/jn.00360.2015.—Contrast, a fundamental feature of visual scenes, is encoded in a distributed manner by ~20 retinal ganglion cell (RGC) types, which stream visual information to the brain. RGC types respond preferentially to positive (ON_{pref}) or negative (OFF_{pref}) contrast and differ in their sensitivity to preferred contrast and responsiveness to nonpreferred stimuli. Vision operates over an enormous range of mean light levels. The influence of ambient illumination on contrast encoding across RGC types is not well understood. Here, we used large-scale multielectrode array recordings to characterize responses of mouse RGCs under lighting conditions spanning five orders in brightness magnitude. We identify three functional RGC types that switch contrast preference in a luminance-dependent manner (Sw1-, Sw2-, and Sw3-RGCs). As ambient illumination increases, Sw1- and Sw2-RGCs shift from ON_{pref} to OFF_{pref} and Sw3-RGCs from OFF_{pref} to ON_{pref}. In all cases, transitions in contrast preference are reversible and track light levels. By mapping spatiotemporal receptive fields at different mean light levels, we find that changes in input from ON and OFF pathways in receptive field centers underlie shifts in contrast preference. Sw2-RGCs exhibit direction-selective responses to motion stimuli. Despite changing contrast preference, direction selectivity of Sw2-RGCs and other RGCs as well as orientation-selective responses of RGCs remain stable across light levels.

ambient illumination; contrast encoding; multielectrode array; retina; switch circuit

THE RETINA MEDIATES VISION on moonless nights and sunny days and in all conditions between these extremes separated in photon flux by a factor of $\sim 10^9$ (Rieke and Rudd 2009). In addition to gain controls in photoreceptors (Burns and Baylor 2001; Fain et al. 2001) and postreceptor circuits (Dunn et al. 2006, 2007), the retina is thought to maintain responsiveness by switching between cell types and pathways optimized to function at different light levels. At the input stage, rods and cones mediate phototransduction in dim and bright environments, respectively. Rod signals reach the inner retina by three alternative pathways that preferentially operate at different light levels (Bloomfield and Dacheux 2001). These pathways converge on some retinal ganglion cell (RGC) types but segregate among others and may give rise to retinal output streams tuned to distinct light levels (Volgyi et al. 2004). Recent studies suggest an important amendment to the notion of functional specialization in the retina. Rather than being turned on and off, it appears that the modus operandi of retinal neurons and pathways can change with ambient illumination. For example, in bright light cones can co-opt rods, inverting their responses via horizontal cells to mediate surround signals (Szikra et al. 2014). Similarly, cones can function as relay cells of rod signals at dim light levels (Nelson 1977; Schneeweis and Schnapf 1995; Soucy et al. 1998; Szikra et al. 2014). AII amacrine cells switch their excitatory input from chemical synapses with rod bipolar cells (RBCs) to electrical synapses with ON cone bipolar cells (Manookin et al. 2008; Munch et al. 2009), whereas RBCs and some RGCs change the source of their inhibitory input (Farrow et al. 2013; Ichinose and Lukasiewicz 2012). The primary rod pathway, rather than saturating, appears to shift from photon counting to contrast encoding with increasing luminance (Ke et al. 2014), and synaptic transmission from bipolar cells transitions from a linear to a rectified regime (Grimes et al. 2014).

Such luminance-dependent changes in neuronal and circuit operation are expected to alter the output of the retina to the brain, which is organized into spike trains of ~20 RGC types. Basic features of visual scenes (e.g., contrast) are encoded in a distributed manner across RGC types, whereas more elaborate features (e.g., motion direction, movement of an object relative to its background) are selectively detected by a few RGC types. Luminance-dependent changes in chromatic, temporal, and spatial tuning of RGCs were identified early in the history of retinal physiology (Barlow et al. 1957; Creutzfeldt and Sakmann 1969; Enroth-Cugell and Lennie 1975; Enroth-Cugell and Robson 1966; Ogawa et al. 1966; Reitner et al. 1991) and have been analyzed in detail since (Farrow et al. 2013; Field et al. 2009; Grimes et al. 2014). By comparison, how contrast encoding and the detection of complex features depend on ambient illumination is not well studied. A recent study found that contrast responses of RGCs can change qualitatively as a function of ambient light levels (Tikidji-Hamburyan et al. 2015). Whether such changes are restricted to specific RGC types that exhibit distinctive shifts in contrast encoding and how altered contrast responses affect the detection of more complex features remain unknown. Here, we used large-scale multielectrode array (MEA) recordings to analyze how the output of the mouse retina varies across ambient illumination conditions spanning five orders of brightness magnitude. We identify three functional RGC types (Sw1-3) that switch their preferred contrast with increasing luminance, two (Sw1- and

Address for reprint requests and other correspondence: D. Kerschensteiner, Dept. of Ophthalmology and Visual Sciences, Washington Univ. School of Medicine, St. Louis, MO 63110 (e-mail: dkerschensteiner@wustl.edu).

Sw2-RGCs) from ON_{pref} to OFF_{pref} and one (Sw3-RGCs) from OFF_{pref} to ON_{pref}. These changes are readily reversible, occur in a specific range of light levels, and result from shifts in the balance of ON and OFF inputs in the receptive field centers of the respective RGCs. Despite changes in their contrast response, Sw2-RGCs, which are direction selective, remain stable across light levels in the strength of their preference and its motion direction, as do other direction- as well as orientation-selective RGCs.

MATERIALS AND METHODS

Animals and tissue preparation. All procedures in this study were approved by the Animal Studies Committee of Washington University School of Medicine and performed in compliance with the National Institutes of Health *Guide for the Care and Use of Laboratory Animals*. Twenty-five- to thirty-five-day-old C57BL/6J mice of both sexes were dark-adapted overnight, deeply anesthetized with CO_2, and killed by cervical dislocation, and their eyes were removed. Retinas were then isolated in cold (4°C) carbogenated mouse artificial cerebrospinal fluid (mACSF) containing (in mM) 125 NaCl, 2.5 KCl, 1.25 Na_2HPO_4, 2 $CaCl_2$, 1 $MgCl_2$, 20 glucose, 26 $NaHCO_3$, and 0.5 L-glutamine. Rectangular pieces (~1 × 1.5 mm) of dorsal retina (Wei et al. 2010) were placed RGC side down on a MEA (Multichannelsystems) and secured by a transparent tissue culture membrane (3-μm pore size, Corning) weighed down by a platinum ring. Enucleation, tissue isolation, and MEA mounting were carried out under infrared illumination (>900 nm).

Multielectrode array recordings. Throughout this study we used MEAs with 252 electrodes arranged in a 16 × 16 grid with the corner positions empty (30-μm electrode size, 100-μm center-center spacing). The tissue was perfused at a rate of 6–8 ml/min with warm (~33°C) mACSF equilibrated with 95% O_2-5% CO_2. Signals of each electrode were band-pass filtered between 300 and 3,000 Hz and digitized at 10 kHz. Signal cutouts from 1 ms before to 2 ms after crossings of negative thresholds (set manually for each channel) were recorded to hard disk together with the time of threshold crossing (i.e., spike time). Principal component analysis of these waveforms was used to sort spikes into trains representing the activity of individual neurons (Offline Sorter, Plexon). Refractory periods were used to assess the quality of the sorting, and only spike trains in which <0.2% of interspike intervals were <2 ms were retained. Cross-correlations among spike trains were used to detect when activity from a single neuron had been recorded on more than one electrode. In these cases, only the train with the most spikes was used for further analysis.

Visual stimulation. Visual stimuli were presented on an organic light emitting display (OLED-XL, eMagin) and focused on retina through a ×20 0.5 NA water immersion objective (Olympus) covering an ~1.7 × 2.3-mm rectangular area. Stimuli were generated in MATLAB with the Cogent Graphics toolbox extensions developed by John Romaya at the LON at the Wellcome Department of Imaging Neuroscience and the display output linearized with custom-written scripts. Neutral density filters were placed in the light path to adjust the mean stimulus intensity over five orders of magnitude [1 rhodopsin isomerization·rod^{-1}·s^{-1} (R*)-10,000 R*]. Mean (maximum) stimulus intensities at the respective light levels were 1 R* (2 R*), 10 R* (20 R*), 100 R* (200 R*), 1,000 R* (2,000 R*), and 10,000 R* (20,000 R*). To probe contrast preference and sensitivity, short (250 ms) full-field luminance steps from the mean intensity were shown every 2.25 s (Fig. 1*A*). Each stimulus presentation consisted of matching steps of opposite polarity (e.g., 5% and −5% contrast). At each light level, different contrasts were shown in 30 pseudorandom sequences. Weber contrast (*C*) of light steps was defined as

$$C = \frac{I - I_b}{I_b}$$

In this, I is the intensity of the step and I_b the intensity between steps. To map spatiotemporal receptive fields, the stimulus display was divided into vertical bars (width: ~50 μm, height: ~1.7 mm). The intensity of each bar was randomly chosen from a Gaussian distribution (RMS contrast: 40%) and updated every 33 ms (refresh rate: 30 Hz) for 30 min. To evaluate direction selectivity, we presented four repeats of drifting full-field square-wave gratings (spatial frequency: 500 μm/cycle, temporal frequency: 1 cycle/s, 8 pseudorandomly chosen directions at 45° intervals). Each stimulus repeat lasted 5 s.

Analysis. Contrast response functions (e.g., Fig. 2*B*) were constructed by measuring the difference between the firing rate in a 250-ms window starting 50 ms after the onset of the respective luminance step (i.e., stimulus window) and the average firing rate of the cell during stimulus sweeps across all presentations of all contrasts. We used a two-alternative forced-choice paradigm to measure contrast thresholds. For every trial of every step the number of spikes observed during the stimulus window was compared to that in a 250-ms window preceding the stimulus. Specifically, we calculated the Poisson probability (P) of the respective spike counts (C) according to

$$P = \frac{e^{-rT} \times (rT)^C}{C!}$$

Here, r is the average firing rate of the cell and T the duration of the stimulus and prestimulus time windows. When the Poisson probability of the stimulus spike count was lower than that of the prestimulus spike count, the step was recorded as detected. Weibull cumulative distribution functions were then fit to the contrast dependence of step detection—separately for negative and positive contrasts–and thresholds defined as the contrast levels at which detection probability reached 75%.

To map spatiotemporal receptive fields and distinguish influences from ON and OFF pathways, we analyzed responses to Gaussian white noise bar stimulation as follows. For each cell, we accumulated stimulus segments preceding each spike, the spike-triggered ensemble (STE). We then calculated the average of the STE, the spike-triggered average (STA). Stimulus bars for which standard deviation in the STA exceeded the average standard deviation of all bars more than threefold were defined as the spatial receptive field of the neuron. We modified a previously described approach to separate influences of ON and OFF pathways in this stimulus area (Gollisch and Meister 2008). For each stimulus bar in the receptive field we identified the first principal component (PC1) of the STE and determined whether its waveform resembled an ON or OFF stimulus. We then separated waveforms in the STE on the basis of their projection onto PC1 into putative ON and OFF components (e.g., for putative ON waveforms the projection is positive for an ON-like PC1) and averaged these groups independently. Next, we evaluated whether these averages separated ON and OFF receptive fields or temporally distinct components of the same polarity. In the latter case, waveforms were combined and the STA judged sufficient to describe the receptive field in this position at this light level. This analysis was repeated for each bar within the spatial receptive field. When ON and OFF receptive fields were observed, we analyzed how many spikes were elicited by ON-dominant vs. OFF-dominant stimuli. In a part of the recording separate from that used to construct receptive fields, the correlations between stimulus segments preceding each spike and ON and OFF receptive fields were calculated to designate spikes as ON or OFF spikes.

To quantify the contrast preference of RGCs at a given light level, we defined a polarity index (PI) as follows:

$$\mathrm{PI} = \frac{R_{ON} - R_{OFF}}{R_{ON} + R_{OFF}}$$

R_{ON} and R_{OFF} represent firing rates to 50% and −50% steps, respectively, for full-field contrast presentation and the numbers of ON and

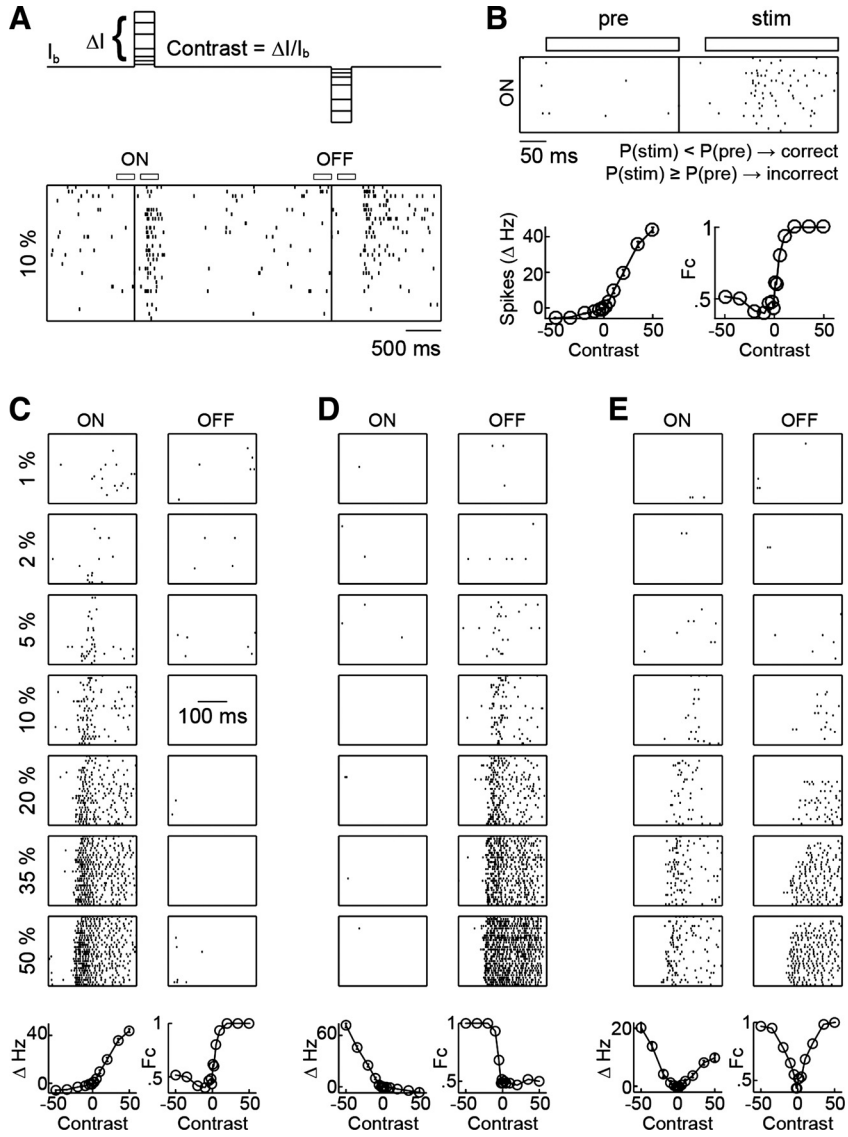

Fig. 1. Characterization of retinal ganglion cell (RGC) contrast responses. *A*, *top*: schematic illustration of the stimulus. *I*, intensity of step; I_b, intensity between steps. *Bottom*: representative spike trains of an ON_{pref} RGC elicited by 30 repeats of the stimulus at ±10% contrast. *B*, *top*: zoomed-in view of the spike train in the prestimulus (pre) and stimulus (stim) window of the 10% contrast light increment. Vertical line indicates stimulus onset. *Bottom*: 2 parameters were used to characterize the spike response to contrast steps. First, the baseline-subtracted average firing rate in the stimulus window was plotted as a function of the contrast of the step (*bottom left*). Second, a 2-alternative forced-choice algorithm comparing the Poisson probabilities of spike counts in the prestimulus and stimulus windows was used to determine detectability of contrast steps based on spike response (see MATERIALS AND METHODS) and the fraction of correct detections (Fc) plotted as a function of step contrast (*bottom right*). *C–E*, *top*: spike trains of representative RGCs, which at 1,000 R* responded exclusively to positive (*C*) or negative (*D*) contrast stimuli or both (*E*). Plots summarizing spike rate responses and contrast detection of the respective cells are shown at *bottom left* and *right*, respectively, in *C–E*.

OFF spikes, respectively, for Gaussian bar white noise stimulation. This index ranges from 1 for a purely ON-responsive cell to −1 for a purely OFF-responsive cell.

To measure direction and orientation preference, the average firing rates of a neuron to each drift direction were computed and the average firing rate in response to interleaved uniform gray stimuli of the same mean luminance subtracted. Direction (DSI) and orientation (OSI) selectivity indexes and preferred stimulus direction and orientations were then calculated based on the circular variance of the response (*R*) as follows:

$$\frac{\sum R(\theta)e^{i\theta}}{\sum R(\theta)} \text{ for DSI}$$

$$\frac{\sum R(\theta)e^{2i\theta}}{\sum R(\theta)} \text{ for OSI}$$

The DSI and OSI are given by the absolute amplitude of the respective values, whereas the preferred direction and orientation are defined by their complex phase (Piscopo et al. 2013). The distribution of DSIs for RGCs switching from ON_{pref} to OFF_{pref} was fit to Gaussian mixture models with varying numbers of components. Using the Bayesian information criterion, a model with two components was found to best fit the data. Based on this model, RGCs switching from ON_{pref} to OFF_{pref} were separated into non-direction-selective Sw1-RGCs and direction-selective Sw2-RGCs. Beyond Sw2-RGCs, direction- and orientation-selective RGCs were identified as neurons with DSI > 0.33 and a combination of OSI > 0.33 and DSI < 0.33, respectively (Piscopo et al. 2013; Zhao et al. 2013).

All analyses were performed with built-in functionality and custom-written programs in MATLAB and R.

Statistics. We used Wilcoxon signed-rank and rank sum tests to compare paired and unpaired sets of continuous quantitative data and χ^2-tests to compare the frequency categorical observations between groups. Throughout the text, population data are summarized by their means ± SE.

RESULTS

Characterizing contrast responses of RGCs. To measure contrast responses of RGCs, short (250 ms) symmetrical steps in full-field light intensity were presented at 2-s intervals (Fig. 1*A*). Weber contrast of this stimulus is defined as the amplitude of the step divided by the intensity between steps (i.e., the mean stimulus intensity). Steps from ±1% to ±50% contrast were shown 30 times, repeated in different pseudorandom

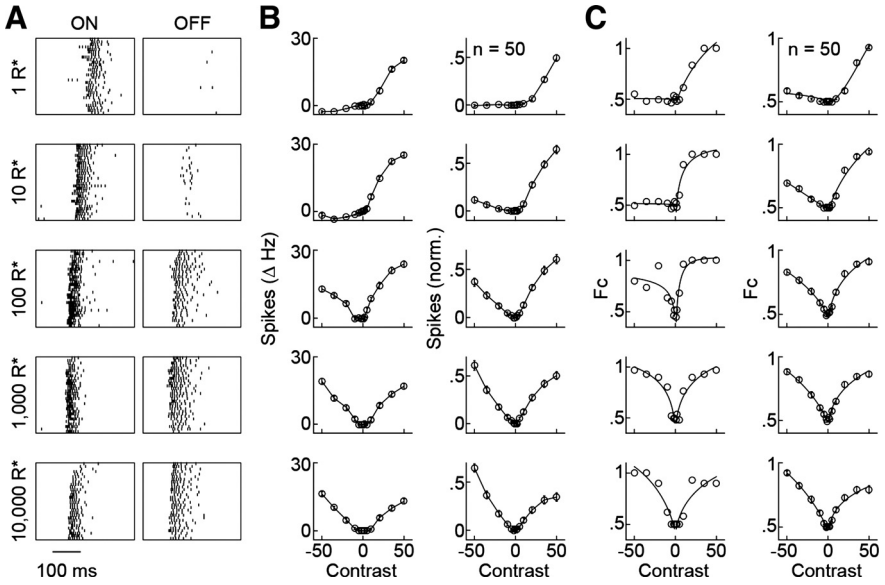

Fig. 2. Luminance-dependent shift in contrast responses of Sw1-RGCs. *A*: spike responses of a representative Sw1-RGC to 50% (ON, *left*) and −50% (OFF, *right*) contrast steps at different mean light levels from 1 R* to 10,000 R*. Spike trains elicited by 30 repeats of each step are shown in 300-ms time windows aligned at the left edge on the onset of the step. *B*: contrast response functions of the spike rate of the representative cell shown in *A* (*left*) and normalized data summarizing all Sw1-RGCs (*right*; $n = 50$, means ± SE). *C*: Fc based on the spike response of the representative Sw1-RGCs in *A* (*left*) and population Fc-contrast response function for all Sw1-RGCs (*right*; means ± SE). Polarity indexes (PIs) of the example cell shown in *A* and summarized in *B* and *C* were −1 at 1 R*, −0.88 at 10 R*, −0.29 at 100 R*, 0.06 at 1,000 R*, and 0.12 at 10,000 R*.

sequences. Contrast response functions of RGCs were then constructed by plotting changes in the average firing rate during a step as a function of its contrast (see MATERIALS AND METHODS, Fig. 1*B*). In addition, we used a two-alternative forced-choice algorithm comparing the Poisson probabilities of prestep and poststep spike trains to assess the ability to detect contrast based on an RGC's response and quantify its threshold(s) (see MATERIALS AND METHODS, Fig. 1*B*).

Typically, RGCs are categorized as ON, OFF, or ON-OFF (Fig. 1, *C–E*) depending on whether they respond to positive contrast, negative contrast, or both, respectively. Because the contrast preference, or polarity, of the RGC types on which we focus in this study changes as a function of ambient illumination, we refer to them at each light level as either ON_{pref} or OFF_{pref} based on the dominant response.

Luminance-dependent shifts in contrast responses of RGCs. To assess the influence of ambient illumination on contrast encoding in the retina, we presented full-field step stimuli (Fig. 1) at five different mean light levels (1 R*·rod^{-1}·s^{-1}, or 1 R* for short, 10 R*, 100 R*, 1,000 R*, 10,000 R*) and recorded responses of large ensembles of RGCs on MEAs. Stimulation at 1 R* and 10 R* activates only rod photoreceptors (scotopic light levels), with signals elicited at 1 R* being transmitted exclusively by RBCs; stimulation at 100 R* and 1,000 R* activates both rods and cones (mesopic light levels); and stimulation at 10,000 R* activates primarily cones (photopic light level) (Bloomfield and Dacheux 2001; Farrow et al. 2013; Field et al. 2009; Murphy and Rieke 2006; Naarendorp et al. 2010; Szikra et al. 2014; Tikidji-Hamburyan et al. 2015).

We restricted our analysis to RGCs that responded reliably at all light levels, indicated by a >70% detection rate of their most preferred contrast step. The majority of these cells (393/511 RGCs, $n = 8$ retinas) showed constant contrast preferences (ON_{pref} or OFF_{pref}, PI, range: 0.099 ± 0.006) across all light levels. However, ~20% of RGCs (108/511) switched polarity as ambient illumination increased. A small number of cells (7/511) exhibited multiple transitions in contrast preference and were not analyzed further. The remaining RGCs (101/511) could be grouped into three functional types (Sw1–Sw3). Sw1-RGCs (50/511) switch from ON_{pref} to OFF_{pref} with increasing luminance (Fig. 2, *A* and *B*; PI at 1 R*: 0.77 ± 0.04, PI at 10,000 R*: −0.25 ± 0.07; $n = 50$, $P < 10^{-5}$). In the scotopic range, sensitivity of Sw1-RGCs to positive contrast increases (Fig. 2*C*; threshold 1 R*: 33.8 ± 1.4%, 10 R*: 21.5 ± 1.6%; $P < 10^{-5}$). Then, as cones are being recruited, Sw1-RGCs begin to respond to negative contrast steps and OFF responses exceed ON responses at photopic light levels. Similar to Sw1-RGCs, Sw2-RGCs (22/511) shift from ON_{pref} to OFF_{pref} with increasing illumination (Fig. 3; PI at 1 R*: 0.62 ± 0.08, PI at 10,000 R*: −0.27 ± 0.11; $n = 22$, $P < 0.002$). While Sw2-RGCs were distinguished from Sw1-RGCs on the basis of their responses to drifting grating stimuli (see Fig. 9), Sw2-RGCs also tend to switch polarity at lower light levels than Sw1-RGCs. Thus ~64% of Sw2-RGCs (14/22) preferred negative contrast at 10 R* compared with only 8% of Sw1-RGCs (4/50, $P < 10^{-5}$). This difference, which was not part of the classification, further supports the notion that Sw1- and Sw2-RGCs are functionally distinct cell types. Contrary to Sw1- and Sw2-RGCs, Sw3-RGCs (29/511) shift from OFF_{pref} to ON_{pref} (Fig. 4; PI at 1 R*: −0.49 ± 0.06, PI at 10,000 R*: 0.71 ± 0.05; $n = 29$, $P < 10^{-4}$). In addition, whereas Sw1- and Sw2-RGCs remain responsive to positive contrast steps in photopic conditions, Sw3-RGCs mostly lose their responses to negative contrast steps.

Shifts in contrast preference of RGCs are reversible. In the experiments described so far, ambient illumination was monotonically increased in $\log_{10}$ steps from 1 R* to 10,000 R*. This raises concerns as to whether the observed shifts in contrast preference could reflect luminance-independent changes in the tissue with increasing duration of the recording, cumulative effects of photoreceptor bleaching, or a combination of both. The following circumstantial evidence argues against these explanations. First, combinations of stimuli shown at each light level differed between recordings, causing the overall duration to vary up to threefold. Despite this, contrast responses of Sw1-, Sw2-, and Sw3-RGCs at specific light levels were consistent across all recordings. Second, shifts in contrast preference were evident by the first stimulus presentation at a new light level, typically shown ~1 min after the increase in illumination, and did not vary consistently as a function of trial

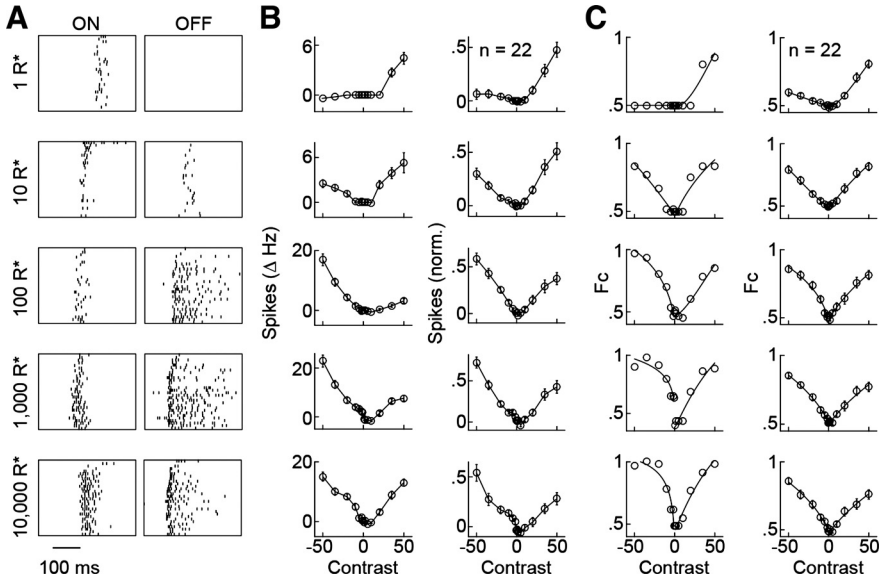

Fig. 3. Luminance-dependent shift in contrast responses of Sw2-RGCs. *A*: spike trains of a representative Sw2-RGC elicited by 50% (ON, *left*) and −50% (OFF, *right*) contrast steps at different mean light levels from 1 R* to 10,000 R*. Responses to 30 repeats of each step are shown in 300-ms time windows aligned at the left edge on the onset of the step. *B*: spike rate-contrast response functions of the representative cell shown in *A* (*left*) and the population of all Sw2-RGCs (*right*; $n = 22$, means ± SE). *C*: Fc-contrast response functions of the representative Sw2-RGCs in *A* (*left*) and the population of all Sw2-RGCs (*right*; means ± SE). PIs of the example cell shown in *A* and summarized in *B* and *C* were −1 at 1 R*, −0.35 at 10 R*, 0.65 at 100 R*, 0.45 at 1,000 R*, and 0.07 at 10,000 R*.

number (Figs. 2–4). Thus PIs calculated from the first and last 5 of 30 trials did not differ significantly from each other for Sw1-, Sw2-, and Sw3-RGCs ($P > 0.7$).

To directly test the reversibility of changes in contrast encoding, we switched ambient illumination back and forth between 10 R* and 1,000 R* and repeated presentations of full-field contrast stimuli at these light levels (Fig. 5*A*). All Sw1-RGCs (Fig. 5*B*; 15/15, $n = 3$ retinas), Sw2-RGCs (Fig. 5*C*; 7/7), and Sw3-RGCs (Fig. 5*D*; 7/7) recorded in these conditions shifted their polarity reversibly. As a result, PIs differed significantly between 10 R* and 1,000 R*, irrespective of which presentations were compared (Sw1-RGCs: $P < 10^{-4}$, Sw2-RGCs: $P < 0.02$, Sw3-RGCs: $P < 0.02$), but not between subsequent stimulations at the same light level (Sw1-RGCs: $P > 0.15$, Sw2-RGCs: $P > 0.5$, Sw3-RGCs: $P > 0.6$). These findings argue strongly that the cell-type-specific changes in contrast encoding of Sw1-, Sw2-, and Sw3-RGCs are the result of luminance-dependent switches in the retinal circuitry, which alter their receptive fields.

Receptive field mechanisms underlying changes in contrast encoding. Two types of receptive field mechanisms could in theory alter the contrast preference of RGCs for full-field stimuli. In RGCs with center-surround receptive fields, changes in the balance of these antagonistic components could shift the polarity of the response. Increases in ambient illumination have been shown to strengthen RGC receptive field surrounds in several species (Barlow et al. 1957; Bisti et al. 1977; Dedek et al. 2008; Enroth-Cugell and Robson 1966; Farrow et al. 2013) and can induce responses to nonpreferred contrasts for large (e.g., full field) stimuli (Creutzfeldt et al. 1970; Sagdullaev and McCall 2005). Alternatively, in RGCs receiving convergent input from ON and OFF pathways, changes in the relative weights of these inputs in the receptive field center could alter contrast preference (Tikidji-Hamburyan et al. 2015). To distinguish between these mechanisms, we characterized spatiotemporal receptive fields of RGCs at light levels from 1 R* to 10,000 R* using Gaussian white noise bar stimulation. Consistently, STAs of Sw1-RGCs (Fig. 6), Sw2-

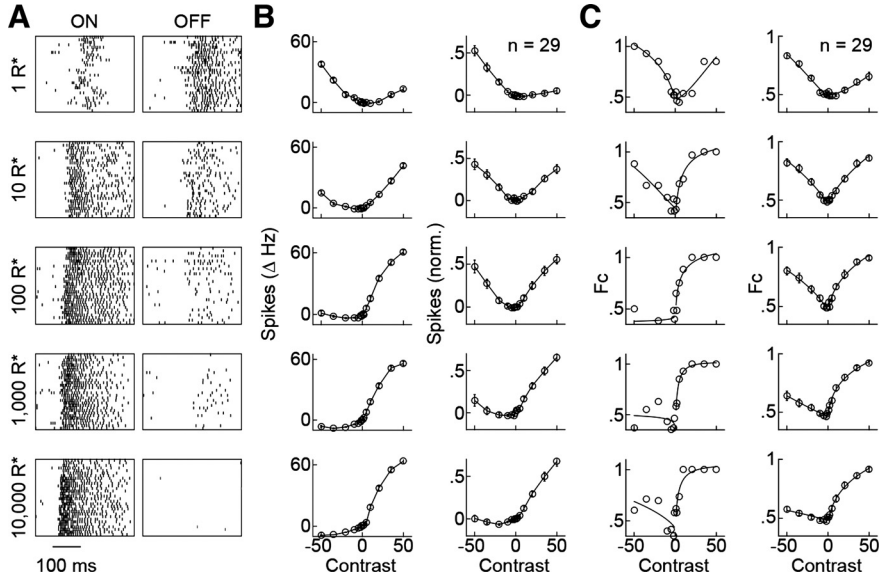

Fig. 4. Luminance-dependent shift in contrast responses of Sw3-RGCs. *A*: spike responses of a representative Sw3-RGC to 50% (ON, *left*) and −50% (OFF, *right*) contrast steps presented at different ambient illumination levels from 1 R* to 10,000 R*. Spike trains elicited by 30 repeats of each step are shown in 300-ms time windows aligned at the left edge on the onset of the step. *B*: contrast response functions of the spike rate of the representative cell shown in *A* (*left*) and summary data for all Sw3-RGCs (*right*; $n = 29$, means ± SE). *C*: Fc based on the spike response of the representative Sw3-RGCs in *A* (*left*) and population Fc-contrast response function for all Sw3-RGCs (*right*; means ± SE). PIs of the example cell shown in *A* and summarized in *B* and *C* were 0.38 at 1 R*, −0.46 at 10 R*, 0.77 at 100 R*, 0.91 at 1,000 R*, and 1 at 10,000 R*.

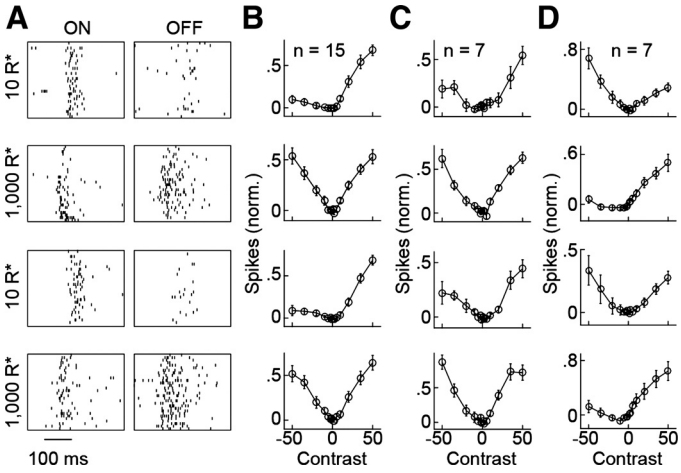

Fig. 5. Contrast preference of Sw1-, Sw2- and Sw3-RGCs switches reversibly and tracks light levels. *A*: representative responses of an Sw2-RGC to ±50% contrast steps presented sequentially at mean light levels of 10 R*, 1,000 R*, 10 R*, and 1,000 R*. *B–D*: summary data of spike rate-contrast response functions of Sw1-RGCs (*B*; $n = 15$, means ± SE), Sw2-RGCs (*C*; $n = 7$), and Sw3-RGCs (*D*; $n = 7$) observed at the respective mean light levels.

RGCs (Fig. 7), and Sw3-RGCs (Fig. 8) showed changes in polarity in their receptive field centers that matched shifts in contrast preference for full-field stimuli, indicating that ambient illumination regulates the balance of convergent ON and OFF pathways impinging on these cells.

To better characterize the transitions between convergent pathways and examine changes in temporal tuning, we separated ON and OFF receptive fields at each light level (see MATERIALS AND METHODS). For Sw1-RGCs, this analysis revealed that, whereas the ON pathway dominates responses at 1 R* and 10 R*, its influence wanes and is superseded by the OFF pathway as cones are being recruited (Fig. 6, *A* and *B*). As a result, a PI based on the strengths of ON and OFF receptive fields (see MATERIALS AND METHODS) switched with increasing luminance (Fig. 6, *A–C*; PI at 1R*: 0.42 ± 0.06, PI at 10,000 R*: −0.51 ± 0.03, $P < 10^{-8}$; $n = 67$ cells, $n = 7$ retinas) similar to the PI calculated for responses to full-field stimulation (Fig. 2). In addition to changes in their relative strengths, temporal sensitivity profiles of ON and OFF receptive fields showed accelerated kinetics with increasing ambient illumination, nearly halving the time by which peak sensitivity precedes a spike [Fig. 6*D*; time to peak for ON and OFF receptive fields (TTP_{ON} and TTP_{OFF}), at 1 R* TTP_{ON}: 182 ± 4 ms, TTP_{OFF}: 187 ± 8 ms, at 10,000 R* TTP_{ON}: 99 ± 2 ms, TTP_{OFF}: 92 ± 2 ms; $P < 10^{-5}$ for comparisons between 1 R* and 10,000 R*].

Receptive field maps of Sw2-RGCs showed transitions in STA polarity, which, similar to those of Sw1-RGCs, were caused by shifts in the balance of ON and OFF inputs in their receptive field center (Fig. 7, *A–C*; PI at 1 R*: 0.22 ± 0.07, PI at 10,000 R*: −0.62 ± 0.04; $P < 10^{-4}$, $n = 27$ cells). In agreement with results from full-field stimulation, switches in

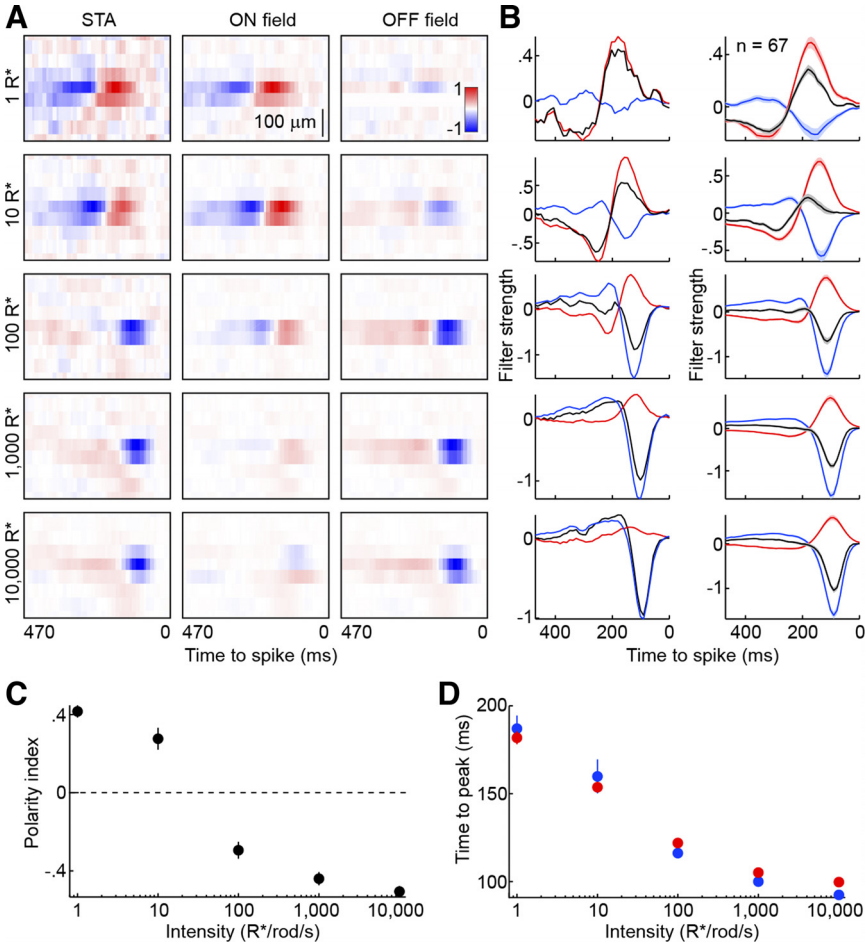

Fig. 6. Luminance-dependent changes in Sw1-RGC receptive fields. *A*: spike-triggered average (STA, *left*), ON (*center*), and OFF (*right*) receptive fields of a representative Sw1-RGC constructed from responses to white noise stimulation at mean light levels from 1 R* to 10,000 R*. Each row corresponds to an ~50-µm-wide bar on the stimulus display. Each column corresponds to an ~10-ms time bin preceding spiking at *time 0*. Spatiotemporal regions of preference for positive and negative contrast are shown in red and blue, respectively. *B*: temporal sensitivity profiles in the center of STA (black trace), ON (red trace), and OFF (blue trace) receptive fields of the representative cell in *A* (*left*) and the population of all Sw1-RGCs (*right*; $n = 67$). For population data the thick line (shaded area) indicates the mean (±SE). *C* and *D*: PI (*C*; means ± SE) and time (*D*; means ± SE) by which peak sensitivities in the center of ON (red) and OFF (blue) receptive fields of Sw1-RGCs precede spikes as a function of mean stimulus intensities.

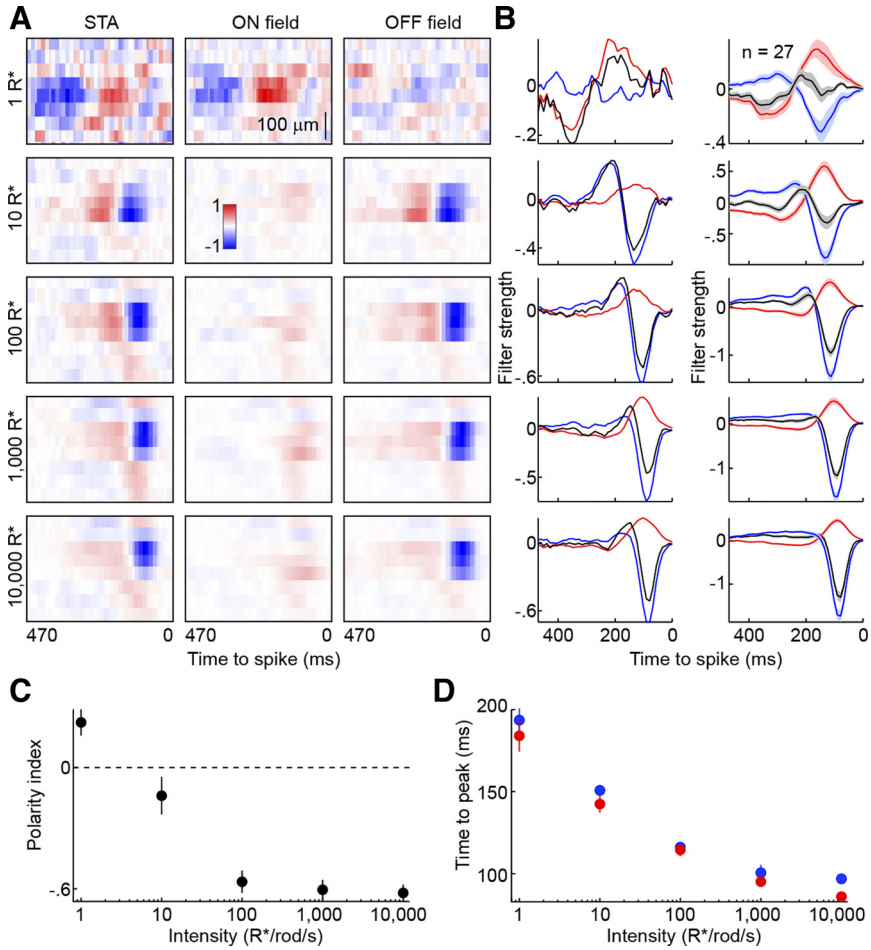

Fig. 7. Luminance-dependent changes in Sw2-RGC receptive fields. *A*: space-time maps of STA (*left*), ON (*center*), and OFF (*right*) receptive fields of a representative Sw2-RGC generated from responses to white noise stimulation at mean light levels from 1 R* to 10,000 R*. Each row corresponds to an ~50-μm-wide bar on the stimulus display. Each column corresponds to an ~10-ms time bin preceding spiking at *time 0*. Regions of preference for positive and negative contrast are shown in red and blue, respectively. *B*: temporal sensitivity profiles in the center of STA (black trace), ON (red trace), and OFF (blue trace) receptive fields of the representative cell in *A* (*left*) and the population of all Sw2-RGCs (*right*; $n = 27$). For population data the thick line (shaded area) indicates the mean (±SE). *C* and *D*: changes in PI (*C*; means ± SE) and time to peak (*D*; means ± SE) for temporal sensitivity profiles of ON (red) and OFF (blue) receptive fields of Sw2-RGCs as a function of mean stimulus intensities.

polarity occurred at lower light levels for Sw2- compared with Sw1-RGCs. Thus ~59% of Sw2-RGCs (16/27) were more sensitive to OFF than ON stimuli in their receptive field center at 10 R* compared with only ~23% of Sw1-RGCs (15/67, $P < 0.002$). Temporal sensitivity profiles of ON and OFF receptive fields were sped up by increases in mean light levels (Fig. 7*D*; at 1 R* TTP_{ON}: 194 ± 8 ms, TTP_{OFF}: 180 ± 9 ms, at 10,000 R* TTP_{ON}: 97 ± 4 ms, TTP_{OFF}: 86 ± 2 ms; $P < 10^{-3}$ for comparisons between 1 R* and 10,000 R*).

STAs of Sw3-RGCs changed polarity in the opposite direction to STAs of Sw1- and Sw2-RGCs. However, similar to the latter, the switches in STA polarity of Sw3-RGCs resulted from shifts in the relative strengths of inputs from ON and OFF pathways in their receptive field center (Fig. 8, *A–C*; PI at 1 R*: −0.32 ± 0.04, PI at 10,000 R*: 0.43 ± 0.05; $P < 10^{-4}$, $n = 29$ cells) and temporal profiles of ON and OFF receptive showed accelerating kinetics with increasing ambient illumination (Fig. 8*D*; at 1 R* TTP_{ON}: 167 ± 10 ms, TTP_{OFF}: 178 ± 7 ms, at 10,000 R* TTP_{ON}: 104 ± 3 ms, TTP_{OFF}: 93 ± 3 ms; $P < 10^{-3}$ for comparisons between 1 R* and 10,000 R*).

Sw2-RGCs are direction selective. To further characterize RGCs that switch contrast preference as a function of ambient illumination, we recorded responses to full-field square-wave gratings (500 μm/cycle, 1 cycle/s, 5 s) drifting in eight directions separated by 45° (Fig. 9*A*). DSIs were calculated based on the circular variance of RGC responses to different drift directions (see MATERIALS AND METHODS). DSIs of RGCs that switch from ON_{pref} to OFF_{pref} formed a bimodal distribution and were best described by a Gaussian mixture model with two components, based on the Bayesian information criterion (McLachlan and Peel 2000). We used this model to separate RGCs switching from ON_{pref} to OFF_{pref} into two functional types: Sw1-RGCs (Fig. 9*A*; DSI: 0.08 ± 0.01; $n = 62$) and Sw2-RGCs (Fig. 9*B*; DSI: 0.54 ± 0.02; $n = 40$, $P < 10^{-16}$). No Sw1-RGCs (0/62) had a DSI > 0.33, and only 5% of Sw2-RGCs (2/40) had a DSI < 0.33, the threshold commonly used to identify direction-selective cells (Piscopo et al. 2013; Zhao et al. 2013). Although the separation of Sw1- and Sw2-RGCs was based on their responses to drifting gratings, Sw2-RGCs also consistently switched contrast preference to full-field and Gaussian white noise bar stimulation at lower light levels than Sw1-RGCs (Figs. 2, 3, 6, 7), supporting their classification as functionally distinct RGC types. DSIs of RGCs switching from OFF_{pref} to ON_{pref} (i.e., Sw3-RGCs) showed a unimodal distribution (Fig. 9*C*; DSI: 0.07 ± 0.01; $n = 38$), and the respective cells were not further subdivided. No Sw3-RGC (0/38) had a DSI > 0.33.

Direction and orientation selectivity are stable over a wide range of light levels. Sw2-RGCs showed direction-selective responses. Conversely, ~30% of direction-selective RGCs (38/124 DSGCs) switched contrast preference in a luminance-dependent manner, indicating that Sw2-RGCs are a subset, possibly one of several identified types, of DSGCs (Borst and Euler 2011; Rivlin-Etzion et al. 2011). To test whether direction selectivity changes as function of ambient illumination, we presented drifting grating stimuli at mean light levels from 1

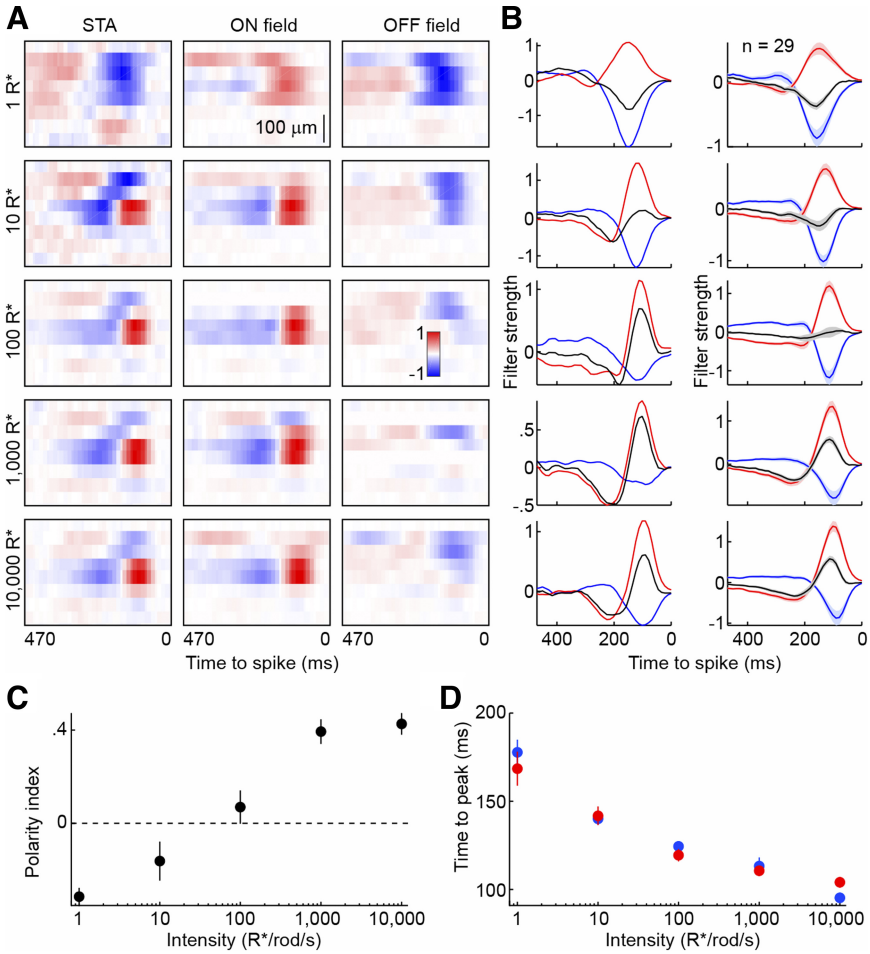

Fig. 8. Luminance-dependent changes in Sw3-RGC receptive fields. *A*: STA (*left*), ON (*center*), and OFF (*right column*) receptive fields for a representative Sw3-RGC constructed from responses to white noise stimulation at mean stimulus light levels from 1 R* to 10,000 R*. Each row corresponds to an ~50-μm-wide bar on the stimulus display. Each column corresponds to an ~10-ms time bin preceding spiking at *time 0*. Spatiotemporal regions of preference for positive and negative contrast are shown in red and blue, respectively. *B*: temporal sensitivity profiles in the center of STA (black trace), ON (red trace), and OFF (blue trace) receptive fields of the representative cell in *A* (*left*) and the population of all Sw3-RGCs (*right*; $n = 29$). For population data the thick line (shaded area) indicates the mean (±SE). *C* and *D*: PI (*C*; means ± SE) and time (*D*; means ± SE) by which peak sensitivities in the center of ON (red) and OFF (blue) receptive fields of Sw3-RGCs precede spikes as a function of mean stimulus intensities.

R* to 10,000 R*. Results from Sw2-RGCs and nonswitching DSGCs were indistinguishable and were therefore combined. Direction tuning was remarkably robust across light levels: the distribution of DSIs did not shift significantly between ambient illumination conditions (Fig. 10*A*; DSI at 1 R*: 0.52 ± 0.04, DSI at 10,000 R*: 0.54 ± 0.03; $P > 0.5$), and the preferred motion direction of each DSGC varied little (Fig. 10*B*).

In agreement with previous studies (He et al. 1998; Venkataramani and Taylor 2010; Zhao et al. 2013), a significant fraction of RGCs (44/578, $n = 5$ retinas) in our recordings responded strongly to opposing motion directions but little to orthogonal stimuli and were therefore referred to as orientation selective (OSGCs). OSGCs, which did not include Sw1-, Sw2-, or Sw3-RGCs, showed stable tuning over the range of light levels tested: distributions of OSIs did not differ significantly (Fig. 10*C*; OSI at 1 R*: 0.45 ± 0.04, OSI at 10,000 R*: 0.45 ± 0.03, $P > 0.4$), and the preferred stimulus orientation of each OSGC stayed within a narrow angular range (Fig. 10*D*). Thus, contrary to changes in encoding of a basic feature (i.e., contrast), detection of more complex features (i.e., motion direction and orientation) was stable across light levels even for RGCs that switched contrast preference (Sw2-RGCs).

DISCUSSION

The retina operates over an enormous range of mean light levels. A fundamental and only partially answered question in vision is how the output of the retina varies across light levels. Spike trains of ~20 RGC types communicate retinal information to the brain. Basic features of visual scenes (e.g., contrast) are encoded in a distributed manner across RGC types, whereas more complex features (e.g., motion direction and orientation) are each detected by one or a few RGC types (Borst and Euler 2011; Munch et al. 2009; Olveczky et al. 2003; Zhang et al. 2012). In this study, we used MEA recordings to analyze how responses of mouse RGCs vary under ambient illumination conditions ranging in brightness from crescent-moonlit nights (1 R*) to overcast days (10,000 R*). We identify three functional RGC types (Sw1-3) that switch their preferred stimulus contrast with increasing mean light levels: two (Sw1- and Sw2-RGCs) from positive to negative and one (Sw3-RGCs) from negative to positive. Switches in contrast preference were reversible and faithfully tracked light levels. Sw2-RGCs exhibit direction-selective responses. We find that, unlike contrast encoding, direction selectivity and orientation selectivity of RGCs are stable across light levels.

Properties and receptive field mechanisms of contrast preference switching. A recent study reported luminance-dependent qualitative changes in contrast responses of RGCs and demonstrated that these changes are conserved across species (mice and pigs) and can be observed in vivo in the dorsolateral geniculate nucleus (dLGN) of the thalamus, a major subcortical target of RGC axons (Tikidji-Hamburyan et al. 2015). However, whether changes in contrast responses are restricted to specific RGC types that undergo distinctive shifts in contrast

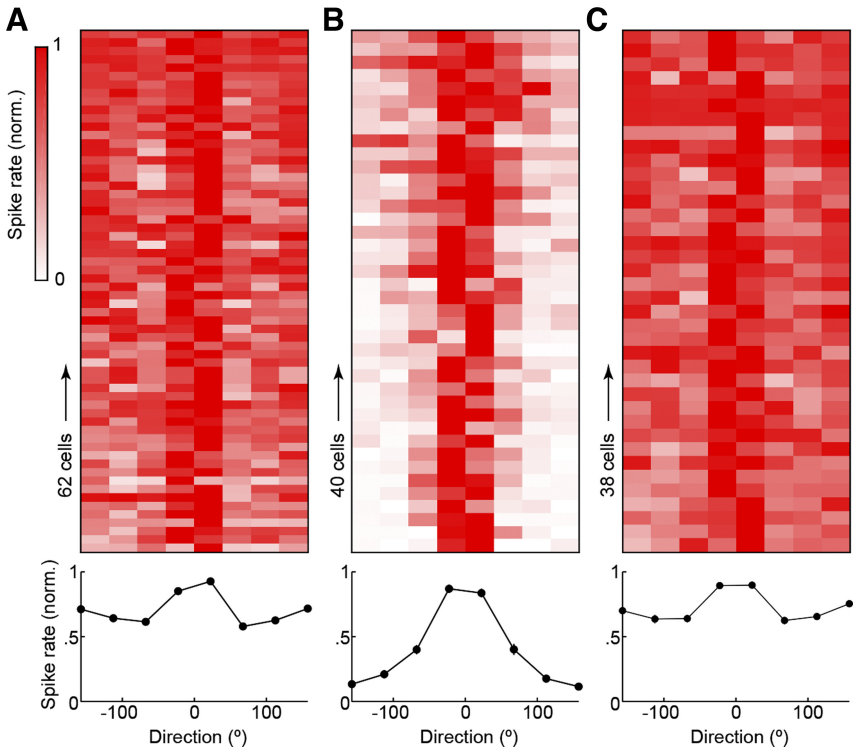

Fig. 9. Sw2-RGCs are direction selective. *A–C*, *top*: colorized plots of the spike responses of Sw1-RGCs (*A*), Sw2-RGCs (*B*), and Sw3-RGCs (*C*) to drifting grating stimuli (see MATERIALS AND METHODS). Each row depicts the response patterns of 1 cell. Responses of all cells were aligned centered on the direction eliciting the maximal responses and its highest-response neighbor. Summary data (means ± SE) of the respective populations are shown at *bottom* of *A* (Sw1-RGCs), *B* (Sw2-RGCs), and *C* (Sw3-RGCs).

encoding remained unknown. Here, we find that the majority of RGCs (~80%) maintain constant contrast preferences across mean light levels from 1 R* to 10,000 R* and identify three functional RGC types that switch preferences (Sw1-3). Sw1- and Sw2-RGCs both convert from ON_{pref} to OFF_{pref} with increasing ambient illumination. Whereas Sw1-RGCs switch preference with the transition from scotopic to mesopic light levels (Figs. 2 and 6), Sw2-RGCs switch within the scotopic range (Figs. 3 and 7). Sw3-RGCs convert in the opposite direction to Sw1- and Sw2-RGCs, from OFF_{pref} to ON_{pref} (Figs. 4 and 8). Thus shifts in contrast encoding are restricted to a few RGC types, which each exhibit specific patterns of change.

When probing contrast encoding, we presented brief light steps (250 ms, Figs. 1–5) to avoid adaptation to luminance levels other than the mean stimulus intensity and restricted our analysis to short-latency responses, which for light increments and decrements arise in ON and OFF pathways, respectively. Inclusion of delayed responses, which arise in opposite pathways to short-latency responses (Demas et al. 2006; Renteria et al. 2006), may account for the greater fraction of RGCs reported to undergo qualitative response changes in the study of Tikidji-Hamburyan et al. (2015).

Surround strengths of some RGC types increase with increasing light levels (Barlow et al. 1957; Bisti et al. 1977; Dedek et al. 2008; Enroth-Cugell and Robson 1966; Farrow et

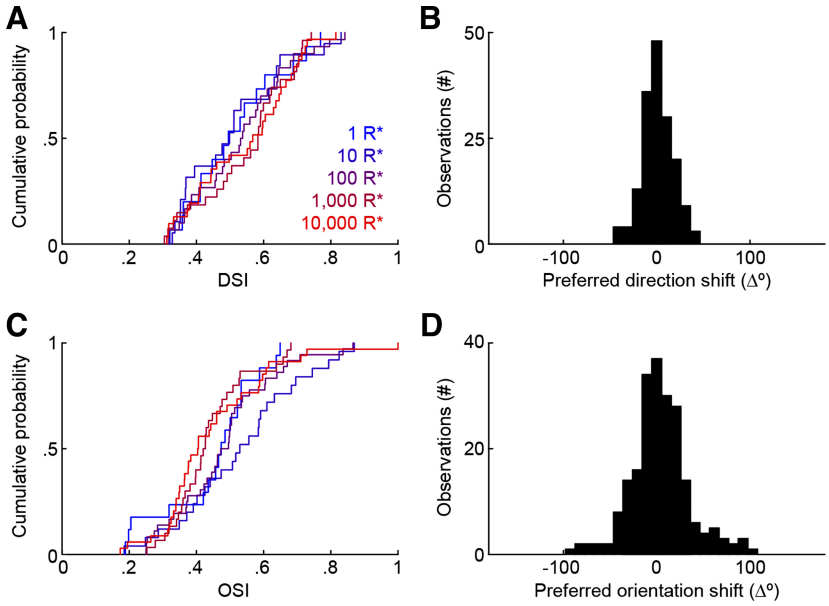

Fig. 10. Direction- and orientation-selective responses of RGCs are stable across light levels. *A*: cumulative distributions of direction selectivity index (DSI) of direction-selective RGCs recorded at light levels from 1 R* to 10,000 R* (color-coded from blue to red as indicated). *B*: population data of differences between angles of preferred motion directions determined for individual RGCs recorded at different light levels. *C* and *D*: analogous to *A* (*C*) and *B* (*D*) for orientation-selective RGCs; OSI, orientation selectivity index.

al. 2013), and shifts in the balance of antagonistic center and surround components of RGC receptive fields can qualitatively alter their responses to full-field stimuli (Creutzfeldt et al. 1970; Sagdullaev and McCall 2005). By mapping spatiotemporal receptive fields at different light levels, we find that this mechanism does not account for the shifting contrast preferences of Sw1-, Sw2-, or Sw3-RGCs. Instead, in all cases (Figs. 6–8) changes in the relative strength of input from ON and OFF pathways in the receptive field center mediate the observed luminance-dependent transitions. Similar changes in convergent ON and OFF input were shown to transiently switch contrast preference (OFF_{pref} to ON_{pref}) in a subset of salamander RGCs after a saccadelike stimulus (Geffen et al. 2007). How ON and OFF pathways converge onto Sw1-, Sw2-, and Sw3-RGCs and how the balance of these convergent inputs shifts as a function of luminance remain to be determined and will likely follow morphological and/or genetic identification of the respective cell types. ON and OFF inputs most commonly converge onto dendrites of bistratified RGCs. Bistratified RGCs include DSGC types (Borst and Euler 2011; Rivlin-Etzion et al. 2011), which in turn include Sw2-RGCs (Fig. 9). However, alternative mechanisms that could mediate ON-OFF convergence on monostratified dendrites have been identified. Some ON bipolar cells form en passant synapses in the OFF sublamina of the inner plexiform layer (IPL) (Dumitrescu et al. 2009; Hoshi et al. 2009; Lauritzen et al. 2013), and input from glutamatergic amacrine cells, which respond to both ON and OFF stimuli, may mediate crossover excitation (Lee et al. 2014).

Unlike changes in contrast preference, which are restricted to a few RGC types undergoing specific transitions, ambient illumination accelerated kinetics of temporal receptive fields in all RGC types, including Sw1-, Sw2-, and Sw3-RGCs (Figs. 6–8). This acceleration is caused by shifts in the influence of rod and cone photoreceptors and shared mechanisms in postreceptor circuits and leads to changes in the temporal tuning of behavioral responses (Field et al. 2009; Umino et al. 2008; Wang et al. 2011).

Direction and orientation selectivity remain stable across light levels. Sw2-RGCs exhibit direction-selective responses and constitute ~30% of DSGCs recorded in our study. Although direction-selective circuits in the retina have been studied in considerable detail (Borst and Euler 2011; Briggman et al. 2011), how ambient illumination influences their function is not well understood. A pair of recent studies showed that DSGCs can switch the direction of their motion preference in response to repeated stimulation (Rivlin-Etzion et al. 2012; Vlasits et al. 2014). These changes in motion preference appear to be caused by shifts in the response polarity of starburst amacrine cells (SACs), critical interneurons presynaptic to DSGCs (Vlasits et al. 2014). Unlike the changes in contrast preference observed in this study, SAC responses were converted gradually and irreversibly by preferential stimulation of receptive field centers (circle: ~225-μm diameter) with bright light (100,000 R*) causing shifts in the balance of rod/center- and cone/surround-driven signals (Vlasits et al. 2014). We find that preferred motion directions of DSGCs remain stable within narrow angular regions under ambient (rectangle: ~1.7 × 2.3 mm) illumination conditions from 1 R* to 10,000 R* (Fig. 10*B*). In addition, the extent of their selectivity was unchanged across light levels (Fig. 10*A*).

RGCs that respond strongly to motion in opposite directions and little to orthogonal stimuli have been observed in several species (Levick and Thibos 1982; Passaglia et al. 2002; Venkataramani and Taylor 2010; Zhao et al. 2013) and were shown to contribute to orientation selectivity in subcortical visual targets of mice (Piscopo et al. 2013; Zhao et al. 2013) where orientation columns were recently observed in superior colliculus (Feinberg and Meister 2015). We find that orientation-selective responses of RGCs remain unchanged in different ambient illumination conditions, both in the extent (i.e., OSI) and the angle of their tuning. Thus, contrary to changes in encoding of a basic feature (i.e., contrast), detection of motion direction and orientation are stable across light levels even for RGCs that switch contrast preference (Sw2-RGCs).

An interesting question emerging from our study is to what end Sw1-, Sw2-, and Sw3-RGCs switch their contrast preference. Answers will have to await future experiments. However, given the stability of Sw2-RGCs in detection of a complex feature (i.e., motion direction), we speculate that changes in contrast preference may in part reflect an adaptive strategy for feature detection that accounts for differences in sources and incident angles of illumination and resulting disparities in contrast of salient features during night and day and transitions between the two (Cronin et al. 2014; Jensen et al. 2001; Undeger 2009).

ACKNOWLEDGMENTS

We thank Dr. Jay Demas and members of the Kerschensteiner lab for helpful discussions and comments on the manuscript.

GRANTS

This work was supported by grants from the Research to Prevent Blindness Foundation (Career Development Award to D. Kerschensteiner and an unrestricted grant to the Dept. of Ophthalmology and Visual Sciences at Washington University) and the National Eye Institute (R01-EY-021855 and R01-EY-023341 to D. Kerschensteiner, T32-EY-013360-13 to J. T. Pearson, and P30-EY-0268 to the Dept. of Ophthalmology and Visual Sciences at Washington University).

DISCLOSURES

No conflicts of interest, financial or otherwise, are declared by the author(s).

AUTHOR CONTRIBUTIONS

Author contributions: J.T.P. and D.K. conception and design of research; J.T.P. and D.K. performed experiments; J.T.P. and D.K. analyzed data; J.T.P. and D.K. interpreted results of experiments; J.T.P. and D.K. prepared figures; J.T.P. and D.K. drafted manuscript; J.T.P. and D.K. edited and revised manuscript; J.T.P. and D.K. approved final version of manuscript.

REFERENCES

Barlow HB, Fitzhugh R, Kuffler SW. Change of organization in the receptive fields of the cat's retina during dark adaptation. *J Physiol* 137: 338–354, 1957.

Bisti S, Clement R, Maffei L, Mecacci L. Spatial frequency and orientation tuning curves of visual neurones in the cat: effects of mean luminance. *Exp Brain Res* 27: 335–345, 1977.

Bloomfield SA, Dacheux RF. Rod vision: pathways and processing in the mammalian retina. *Prog Retin Eye Res* 20: 351–384, 2001.

Borst A, Euler T. Seeing things in motion: models, circuits, and mechanisms. *Neuron* 71: 974–994, 2011.

Briggman KL, Helmstaedter M, Denk W. Wiring specificity in the direction-selectivity circuit of the retina. *Nature* 471: 183–188, 2011.

Burns ME, Baylor DA. Activation, deactivation, and adaptation in vertebrate photoreceptor cells. *Annu Rev Neurosci* 24: 779–805, 2001.

Creutzfeldt O, Sakmann B. Neurophysiology of vision. *Annu Rev Physiol* 31: 499–544, 1969.

Creutzfeldt OD, Sakmann B, Scheich H, Korn A. Sensitivity distribution and spatial summation within receptive-field center of retinal on-center ganglion cells and transfer function of the retina. *J Neurophysiol* 33: 654–671, 1970.

Cronin TW, Johnson S, Marshall NJ, Warrant EJ. *Visual Ecology*. Princeton, NJ: Princeton Univ. Press, 2014.

Dedek K, Pandarinath C, Alam NM, Wellershaus K, Schubert T, Willecke K, Prusky GT, Weiler R, Nirenberg S. Ganglion cell adaptability: does the coupling of horizontal cells play a role? *PloS One* 3: e1714, 2008.

Demas J, Sagdullaev BT, Green E, Jaubert-Miazza L, McCall MA, Gregg RG, Wong RO, Guido W. Failure to maintain eye-specific segregation in nob, a mutant with abnormally patterned retinal activity. *Neuron* 50: 247–259, 2006.

Dumitrescu ON, Pucci FG, Wong KY, Berson DM. Ectopic retinal ON bipolar cell synapses in the OFF inner plexiform layer: contacts with dopaminergic amacrine cells and melanopsin ganglion cells. *J Comp Neurol* 517: 226–244, 2009.

Dunn FA, Doan T, Sampath AP, Rieke F. Controlling the gain of rod-mediated signals in the Mammalian retina. *J Neurosci* 26: 3959–3970, 2006.

Dunn FA, Lankheet MJ, Rieke F. Light adaptation in cone vision involves switching between receptor and post-receptor sites. *Nature* 449: 603–606, 2007.

Enroth-Cugell C, Lennie P. The control of retinal ganglion cell discharge by receptive field surrounds. *J Physiol* 247: 551–578, 1975.

Enroth-Cugell C, Robson JG. The contrast sensitivity of retinal ganglion cells of the cat. *J Physiol* 187: 517–552, 1966.

Fain GL, Matthews HR, Cornwall MC, Koutalos Y. Adaptation in vertebrate photoreceptors. *Physiol Rev* 81: 117–151, 2001.

Farrow K, Teixeira M, Szikra T, Viney TJ, Balint K, Yonehara K, Roska B. Ambient illumination toggles a neuronal circuit switch in the retina and visual perception at cone threshold. *Neuron* 78: 325–338, 2013.

Feinberg EH, Meister M. Orientation columns in the mouse superior colliculus. *Nature* 519: 229–232, 2015.

Field GD, Greschner M, Gauthier JL, Rangel C, Shlens J, Sher A, Marshak DW, Litke AM, Chichilnisky EJ. High-sensitivity rod photoreceptor input to the blue-yellow color opponent pathway in macaque retina. *Nat Neurosci* 12: 1159–1164, 2009.

Geffen MN, de Vries SE, Meister M. Retinal ganglion cells can rapidly change polarity from Off to On. *PLoS Biol* 5: e65, 2007.

Gollisch T, Meister M. Modeling convergent ON and OFF pathways in the early visual system. *Biol Cybern* 99: 263–278, 2008.

Grimes WN, Schwartz GW, Rieke F. The synaptic and circuit mechanisms underlying a change in spatial encoding in the retina. *Neuron* 82: 460–473, 2014.

He S, Levick WR, Vaney DI. Distinguishing direction selectivity from orientation selectivity in the rabbit retina. *Vis Neurosci* 15: 439–447, 1998.

Hoshi H, Liu WL, Massey SC, Mills SL. ON inputs to the OFF layer: bipolar cells that break the stratification rules of the retina. *J Neurosci* 29: 8875–8883, 2009.

Ichinose T, Lukasiewicz PD. The mode of retinal presynaptic inhibition switches with light intensity. *J Neurosci* 32: 4360–4371, 2012.

Jensen HW, Durand F, Dorsey J, Stark MM, Shirley P, Premo S. A physically-based night sky model. In: *Proceedings of the 28th Annual Conference on Computer Graphics and Interactive Techniques*. New York: ACM, 2001, p. 399–408.

Ke JB, Wang YV, Borghuis BG, Cembrowski MS, Riecke H, Kath WL, Demb JB, Singer JH. Adaptation to background light enables contrast coding at rod bipolar cell synapses. *Neuron* 81: 388–401, 2014.

Lauritzen JS, Anderson JR, Jones BW, Watt CB, Mohammed S, Hoang JV, Marc RE. ON cone bipolar cell axonal synapses in the OFF inner plexiform layer of the rabbit retina. *J Comp Neurol* 521: 977–1000, 2013.

Lee S, Chen L, Chen M, Ye M, Seal RP, Zhou ZJ. An unconventional glutamatergic circuit in the retina formed by vGluT3 amacrine cells. *Neuron* 84: 708–715, 2014.

Levick WR, Thibos LN. Analysis of orientation bias in cat retina. *J Physiol* 329: 243–261, 1982.

Manookin MB, Beaudoin DL, Ernst ZR, Flagel LJ, Demb JB. Disinhibition combines with excitation to extend the operating range of the OFF visual pathway in daylight. *J Neurosci* 28: 4136–4150, 2008.

McLachlan G, Peel D. *Finite Mixture Models*. Hoboken, NJ: Wiley, 2000.

Munch TA, da Silveira RA, Siegert S, Viney TJ, Awatramani GB, Roska B. Approach sensitivity in the retina processed by a multifunctional neural circuit. *Nat Neurosci* 12: 1308–1316, 2009.

Murphy GJ, Rieke F. Network variability limits stimulus-evoked spike timing precision in retinal ganglion cells. *Neuron* 52: 511–524, 2006.

Naarendorp F, Esdaille TM, Banden SM, Andrews-Labenski J, Gross OP, Pugh EN Jr. Dark light, rod saturation, and the absolute and incremental sensitivity of mouse cone vision. *J Neurosci* 30: 12495–12507, 2010.

Nelson R. Cat cones have rod input: a comparison of the response properties of cones and horizontal cell bodies in the retina of the cat. *J Comp Neurol* 172: 109–135, 1977.

Ogawa T, Bishop PO, Levick WR. Temporal characteristics of responses to photic stimulation by single ganglion cells in the unopened eye of the cat. *J Neurophysiol* 29: 1–30, 1966.

Olveczky BP, Baccus SA, Meister M. Segregation of object and background motion in the retina. *Nature* 423: 401–408, 2003.

Passaglia CL, Troy JB, Ruttiger L, Lee BB. Orientation sensitivity of ganglion cells in primate retina. *Vision Res* 42: 683–694, 2002.

Piscopo DM, El-Danaf RN, Huberman AD, Niell CM. Diverse visual features encoded in mouse lateral geniculate nucleus. *J Neurosci* 33: 4642–4656, 2013.

Reitner A, Sharpe LT, Zrenner E. Is colour vision possible with only rods and blue-sensitive cones? *Nature* 352: 798–800, 1991.

Renteria RC, Tian N, Cang J, Nakanishi S, Stryker MP, Copenhagen DR. Intrinsic ON responses of the retinal OFF pathway are suppressed by the ON pathway. *J Neurosci* 26: 11857–11869, 2006.

Rieke F, Rudd ME. The challenges natural images pose for visual adaptation. *Neuron* 64: 605–616, 2009.

Rivlin-Etzion M, Wei W, Feller MB. Visual stimulation reverses the directional preference of direction-selective retinal ganglion cells. *Neuron* 76: 518–525, 2012.

Rivlin-Etzion M, Zhou K, Wei W, Elstrott J, Nguyen PL, Barres BA, Huberman AD, Feller MB. Transgenic mice reveal unexpected diversity of on-off direction-selective retinal ganglion cell subtypes and brain structures involved in motion processing. *J Neurosci* 31: 8760–8769, 2011.

Sagdullaev BT, McCall MA. Stimulus size and intensity alter fundamental receptive-field properties of mouse retinal ganglion cells in vivo. *Vis Neurosci* 22: 649–659, 2005.

Schneeweis DM, Schnapf JL. Photovoltage of rods and cones in the macaque retina. *Science* 268: 1053–1056, 1995.

Soucy E, Wang Y, Nirenberg S, Nathans J, Meister M. A novel signaling pathway from rod photoreceptors to ganglion cells in mammalian retina. *Neuron* 21: 481–493, 1998.

Szikra T, Trenholm S, Drinnenberg A, Juttner J, Raics Z, Farrow K, Biel M, Awatramani G, Clark DA, Sahel JA, da Silveira RA, Roska B. Rods in daylight act as relay cells for cone-driven horizontal cell-mediated surround inhibition. *Nat Neurosci* 17: 1728–1735, 2014.

Tikidji-Hamburyan A, Reinhard K, Seitter H, Hovhannisyan A, Procyk CA, Allen AE, Schenk M, Lucas RJ, Munch TA. Retinal output changes qualitatively with every change in ambient illuminance. *Nat Neurosci* 18: 66–74, 2015.

Umino Y, Solessio E, Barlow RB. Speed, spatial, and temporal tuning of rod and cone vision in mouse. *J Neurosci* 28: 189–198, 2008.

Undeger C. Modeling daytime and night illumination. In: *Proceedings of the 2009 Summer Computer Simulation Conference*. Istanbul, Turkey: Society for Modeling Simulation International, 2009, p. 33–39.

Venkataramani S, Taylor WR. Orientation selectivity in rabbit retinal ganglion cells is mediated by presynaptic inhibition. *J Neurosci* 30: 15664–15676, 2010.

Vlasits AL, Bos R, Morrie RD, Fortuny C, Flannery JG, Feller MB, Rivlin-Etzion M. Visual stimulation switches the polarity of excitatory input to starburst amacrine cells. *Neuron* 83: 1172–1184, 2014.

Volgyi B, Deans MR, Paul DL, Bloomfield SA. Convergence and segregation of the multiple rod pathways in mammalian retina. *J Neurosci* 24: 11182–11192, 2004.

Wang YV, Weick M, Demb JB. Spectral and temporal sensitivity of cone-mediated responses in mouse retinal ganglion cells. *J Neurosci* 31: 7670–7681, 2011.

Wei W, Elstrott J, Feller MB. Two-photon targeted recording of GFP-expressing neurons for light responses and live-cell imaging in the mouse retina. *Nat Protoc* 5: 1347–1352, 2010.

Zhang Y, Kim IJ, Sanes JR, Meister M. The most numerous ganglion cell type of the mouse retina is a selective feature detector. *Proc Natl Acad Sci USA* 109: E2391–E2398, 2012.

Zhao X, Chen H, Liu X, Cang J. Orientation-selective responses in the mouse lateral geniculate nucleus. *J Neurosci* 33: 12751–12763, 2013.